Size-Dependent Charge Transfer in Blends of PbS Quantum Dots with a Low-Gap Silicon-Bridged Copolymer

Grigorios Itskos,* Paris Papagiorgis, Demetra Tsokkou, Andreas Othonos,
Felix Hermerschmidt, Solon P. Economopoulos, Maksym Yarema, Wolfgang Heiss,
and Stelios Choulis

The photophysics of bulk heterojunctions of a high-performance, low-gap silicon-bridged dithiophene polymer with oleic acid capped PbS quantum dots (QDs) are studied to assess the material potential for light harvesting in the visible- and IR-light ranges. By employing a wide range of nanocrystal sizes, systematic dependences of electron and hole transfer on quantum-dot size are established for the first time on a low-gap polymer–dot system. The studied system exhibits type II band offsets for dot sizes up to ca. 4 nm, whch allow fast hole transfer from the quantum dots to the polymer that competes favorably with the intrinsic QD recombination. Electron transfer from the polymer is also observed although it is less competitive with the fast polymer exciton recombination for most QD sizes studied. The incorporation of a fullerene derivative provides efficient electron-quenching sites that improve interfacial polymer-exciton dissociation in ternary polymer–fullerene–QD blends. The study indicates that programmable band offsets that allow both electron and hole extraction can be produced for efficient light harvesting based on this low-gap polymer-PbS QD composite.

1. Introduction

Organic semiconductor bulk heterojunction solar cells have seen unprecedented progress during the last 15 years, overcoming several key obstacles, and achieving more than two orders of magnitude efficiency increase towards the anticipated milestone solar cell efficiency of 10%.[1,2] Equally impressive has been the progress in light harvesting based on colloidal quantum dots (QDs) with successful demonstrations based on all-QD active regions of Schottky[3,4] solar cells and recently of depleted heterojunction[5] and p–n junction[6] types of devices. While high-performance light sensors can be produced based on fully organic or fully nanocrystal active regions, composites of the two systems exhibit important advantages. Organic devices can benefit from the higher absorption of nanocrystals (NCs) compared to the fullerene acceptors, size-tunable levels to tailor band-offsets, control over NC shape to optimize composite morphologies, and the possibility of higher stability arising from the incorporation of a less-volatile inorganic moiety. For QD devices an extended network of highly absorbing conducting organic components can significantly enhance light harvesting and can provide pathways for efficient charge, energy, and even multiexciton extraction.[7,8]

The seminal proposal by Alivisatos and co-workers[9] to replace fullerenes with colloidal quantum dots (QDs) as the acceptor material in organic bulk heterojunctions (BHJs) paved the way for hybrid polymer–nanocrystal structures. Research on hybrid PVs intensified with the publication of another article by the same group demonstrating a power conversion efficiency (PCE) of over 2% by using a mixture of CdSe NCs and P3HT as the active layer in a BHJ architecture.[10] Numerous reports followed, i.e. see recent reviews,[11,12] mainly based on Cd chalcogenide quantum dots and phenylenevinylene (PPV) and polythiophene (P3HT) conjugated polymers. Control over blend nanomorphology[11–15] and the shape and aspect ratio of the NCs[11–13,16] has proven to be critical in improving performance. A further increase in efficiency was enabled by two important developments: i) the use of mild postfabrication chemical treatments to replace bulky insulating QD ligands with shorter capping molecules to allow better charge extraction[15–20] and ii) the employment of new low-bandgap copolymers.[15–22]

Prof. G Itskos, P. Papagiorgis
Department of Physics
Experimental Condensed Matter Physics Laboratory
University of Cyprus
Nicosia, 1678, Cyprus
E-mail: itskos@ucy.ac.cy

Dr. D. Tsokkou, Prof. A. Othonos
Department of Physics
Research Center of Ultrafast Science
University of Cyprus
Nicosia, 1678, Cyprus

F. Hermerschmidt, Dr. S. P. Economopoulos, Prof. S. Choulis
Molecular Electronics and Photonics Research Unit
Department of Mechanical Engineering
and Materials Science and Engineering
Cyprus University of Technology
Limassol 3603, Cyprus

Dr. M. Yarema, Prof. W. Heiss
Institute of Semiconductor and Solid State Physics
University of Linz
Linz, 4040, Austria

FULL PAPER

Despite the undoubted successes of Cd chalcogenide based-structures, the employment of lower gap QDs to harvest a greater fraction of the solar spectrum or to enable IR detection for a plethora of required applications, while reducing IR heating effects, is highly attractive. Perhaps the most promising such material is PbS, owing to its unique electronic properties and mature chemistry.[23] Early successes using PbS QD–polythiophenes or fullerene binary materials have been reported in photodetectors, with impressive results of high external quantum efficiency (EQE) values up to 50% and sensitivity up to 1800 nm being demonstrated recently with ternary blends of the aforementioned materials.[24] However extensive efforts by our group to produce efficient solar cells based on such P3HT-based ternary approaches were discouraging with best power conversion efficiencies/external quantum efficiencies at the low level of ca. 0.2%/5%, respectively. Overall and despite expectations, PbS QD–organic solar cells based on conventional polymer donors have vastly underperformed compared to all-PbS QD and all-organic devices.[11,12] The breakthrough came from the use of a low-gap polymer that allowed Ginger and co-workers[22] to demonstrate significantly higher efficiencies of 0.55%. By benefitting from the employment of postfabrication ligand-exchange treatments, a further efficiency leap to respectable levels of 3–4% was recently demonstrated.[17–20]

The common denominator in all recent efficient efforts employing PbS or other types of colloidal QDs in such hybrid devices was the employment of a low-gap copolymer as the electron-donor material. Better energy-level alignment, improved morphology, and higher hole mobilities leading to a better electron–hole transport balance may have been some of the reasons for the better performance, however more fundamental studies are needed to shed light on such attributes and provide the necessary feedback for device optimization. A handful of studies investigating the photophysics of bulk blends of QDs–low-gap polymers exist in the literature with just two of them reporting on charge-transfer dynamics at the polymer–PbS QD interface.[17,20] Importantly no studies on the influence of QD size on charge extraction have been reported, and other important experimental parameters such as excitation energy and fluence have remained unexplored.

We have performed a systematic spectroscopic investigation of blend heterojunctions of the low-bandgap silicon-bridged dithiophene copolymer poly[(4,40-bis(2-ethylhexyl)dithieno[3,2-b:20,30-d]silole)-2,6-diylalt-(2,1,3-benzothiadiazole)-4,7-diyl], known as Si–PCPDTBT,[25] with various oleic acid capped PbS QDs absorbing in a wide range from 900–2000 nm. Si–PCPDTBT is a new and highly promising copolymer donor material for light harvesting. It exhibits a near-infrared bandgap and HOMO–LUMO levels in the optimum predicted ranges for polymer donors in BHJ solar cells,[26] high hole mobilities up to 10^{-2} cm^2 V^{-1} s^{-1},[27] and a proven ability in the realization of high-performance polymer–fullerene solar cells.[25,27] Furthermore the presence of the central Si-bridge atom ensures good environmental stability;[28] this property seems to be supported by preliminary results of our ongoing photodegradation studies, which show high air-stability of blend films of Si–PCPDTBT with PbS nanocrystals. Importantly the material can form type II band offsets with some of the aforementioned QD sizes, which makes the blend suitable for light harvesting. Our work

reports on the first attempt at blending the promising polymer with a different acceptor material than fullerenes, to assess the new composite's potential for hybrid devices.

Electrochemistry with optical absorption was employed to provide precise measurements of the electronic levels of the studied materials, while a combination of steady-state and time-resolved luminescence and transmission allowed us to probe the dynamics of the charge-extraction process across a wide temporal range (200 fs–200 ns). The data show signatures of electron- and hole-transfer processes originating in the polymer/QD component respectively. Charge transfer is found to be strongly dependent on QD size with efficient hole transfer obtained from small QDs. Electron transfer for most NC sizes studied appears less efficient than that of the intrinsic Si–PCPDTBT recombination as indicated by the incomplete polymer exciton quenching. The incorporation of a fullerene derivative was found to provide efficient electron-quenching sites and improve polymer exciton dissociation in ternary polymer–fullerene–QD blends.

2. Results and Discussion

2.1. Optical Absorption

Normalized absorbance of the QD solutions used in the study is displayed in **Figure 1**a. Tuning of the QD size is evidenced by the wide spectral tuning of the 1s interband QD transition in the 900–2000 nm infrared region. Seven different QDs were employed with diameters in the range 2.9–9.2 nm, see **Table 1**, estimated from the absorption peaks and the sizing curve given in reference [29]. The employed sizes allow a wide tuning of the QD levels and enable investigations of both type II and type I polymer–QD band alignments. Along with the seven binary films, three ternary Si–PCPDTBT:PCBM:PbS QD blends based on the ca. 2.9, 4.3, and 6.8 nm QDs were also studied. Figure 1b contains absorption-coefficient data in logarithmic scale from a pristine PbS QD, a pristine Si–PCPDTBT, and the respective hybrid film. The polymer exhibits a strong, structured absorbance extending to the infrared up to ca. 850–900 nm that has been attributed to the strong π stacking of the polymer chains.[25] The 1s absorption peak of the QD film is clearly visible at ca. 1165 nm. Absorption in the hybrid film is a convolution of the polymer and QD contributions. Light harvesting in the ca. 550–800 nm range is dominated by the polymer and QD interband transitions prevail in the infrared, while both materials contribute at shorter wavelengths than 500 nm.

2.2. Electrochemistry

HOMO and LUMO levels (valence-band and conduction-band minimum, respectively) of the quantum dot solutions were measured by electrochemistry. The same solutions were used for the optical characterization studies, which allowed precise determination of the materials' band offsets and enabled a reliable interpretation of the spectroscopic data. The energies of four different QD-size solutions were determined with an uncertainty of ±0.1 eV, from the onset of the respective peaks in the cyclic
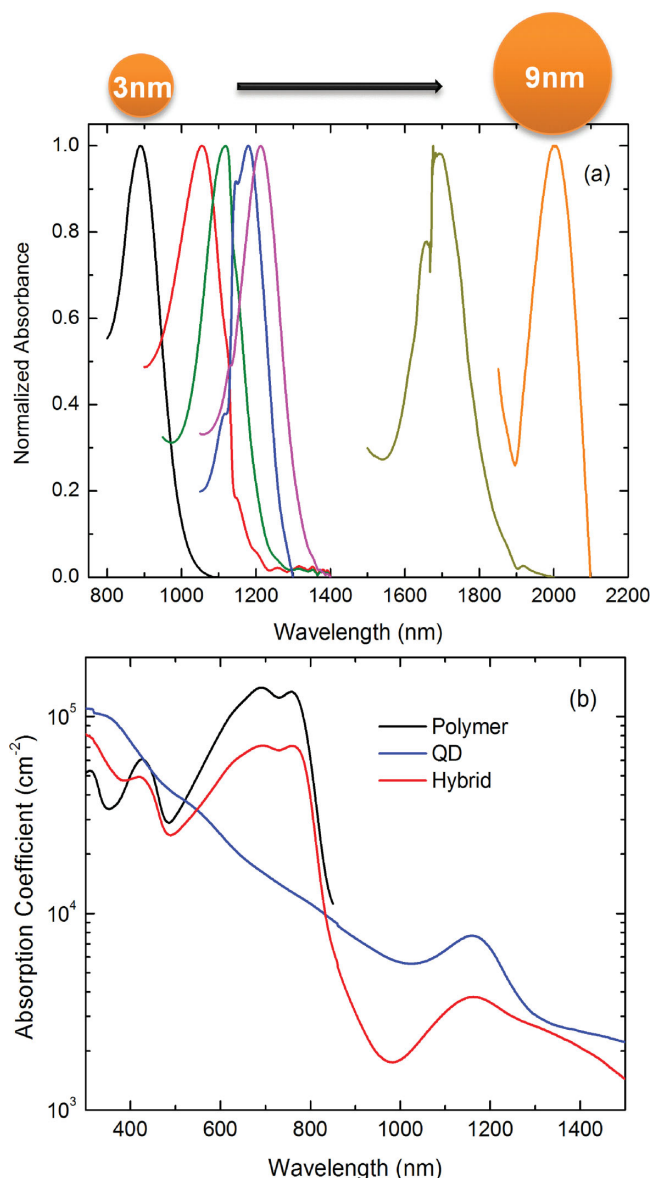
Figure 1. a) Normalized absorbance of the various PbS QDs in chlorobenzene, used in the study demonstrating the wide spectral tuning of the 1s QD transition in the 900–2000 nm infrared region. b) Absorption coefficient in logarithmic scale from a pristine QD, a Si–PCPDTBT, and the respective hybrid film.

voltammetry (CV) spectra. **Figure 2** contains CV data from the ca. 4.3 and 3.8 nm QDs. The former exhibits an oxidation process at about 0.25 V with a step onset of ca. 0.1 V yielding a HOMO level of −5.20 eV. A reversible reduction process is observed at about −0.9 V with an onset at around −0.70 V from which a LUMO of −4.40 eV is estimated. For the second solution, using a similar process, HOMO/LUMO levels of −5.30/−4.30 eV were obtained, respectively. A rough estimation of the HOMO/LUMO was also obtained by using the following equations:

$$E_{HOMO} = -[5.0 + (E_{1S} - E_{PbS})/2](eV),$$
$$E_{LUMO} = -[4.6 - (E_{1S} - E_{PbS})/2](eV) \tag{1}$$

where E_{1s} represents the absorption peak energy of the QD solutions obtained by steady-state absorbance and −5.0/−4.6 eV are the HOMO/LUMO values of bulk PbS.[30] The estimation assumes equal sharing of the excess confinement energy between the QDs' conduction and valence bands. Interestingly the rather simplistic calculation yields HOMO/LUMO values that agree with the CV data to within the ±0.1 eV margin of error of the CV experiment. The good agreement between the two techniques indicates that their combination is a reliable tool for the determination of the materials' energy levels. A summary of the results from the absorption and electrochemical measurements in the QD materials is displayed in Table 1.

Based on the measurements and HOMO–LUMO values of the Si–PCPDTBT[25] and PCBM[24] from the literature, the energy-level diagram of the three materials employed in our studies is drawn in **Figure 3**. Type II polymer–dot heterostructures suitable for light-harvesting devices are expected to be formed for QD sizes smaller than about 4–4.5 nm with a transition to type I band alignment for larger dots. In the former structures, the energetics allow for electron and hole photoinduced transfer that originates in the polymer/QD component, respectively. Upon addition of PCBM to form ternary blends, additional electron-transfer channels from the polymer and the QDs towards the fullerene become available.

2.3. Pump–Probe Transmission

Pump–probe transmission was employed to study the dynamics of photogenerated species in pristine and blend films at ultrafast scales down to 200 fs. The technique allows probing of both excitons and polarons that are either fluorescent

Table 1. Summary of the absorption and electrochemical measurements of QD materials.

Absorption[a] [±5 nm]	890		1055	1120		1175		1215		1690	2000
Estimated QD size[b] [±0.5 nm]	2.9		3.5	3.8		4.0		4.3		6.8	9.2
E_{HOMO} [±0.1 eV]	5.40[c]		5.50[d]	5.40[c]		5.30[c]	5.35[d]	5.25[c]	5.30[d]	5.20[c]	5.30[d]	5.15[c]	5.10[c]
E_{LUMO} [±0.1 eV]	4.20[c]		4.10[d]	4.20[c]		4.35[c]	4.25[d]	4.20[c]	4.25[d]	4.40[c]	4.30[d]	4.45[c]	4.50[c]

[a]Energy gap obtained from the 1s absorption of the QDs in chlorobenzene; [b]QD size estimated by the sizing curve of reference [29]; [c]Energy levels measured by cyclic voltammetry; [d]Energy levels measured by optical absorption (see text).
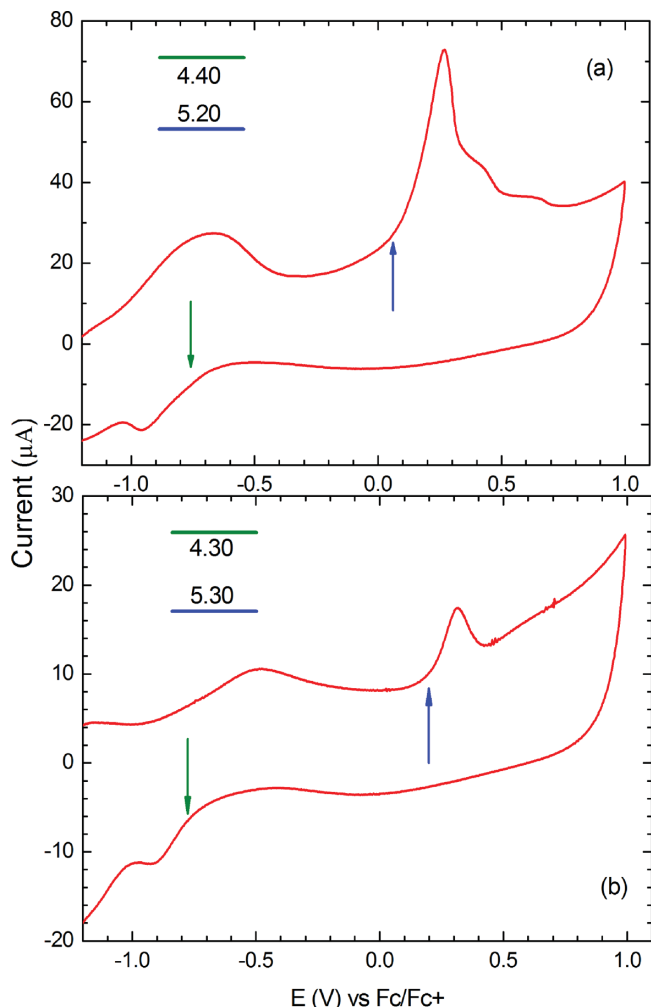
Figure 2. Cyclic voltammetry data from a) the ca. 4.3 nm and b) 3.8 nm QDs. The arrows denote the approximate onsets of oxidation (blue) and reduction (green) steps from which the HOMO and LUMO levels of the nanocrystals are obtained.
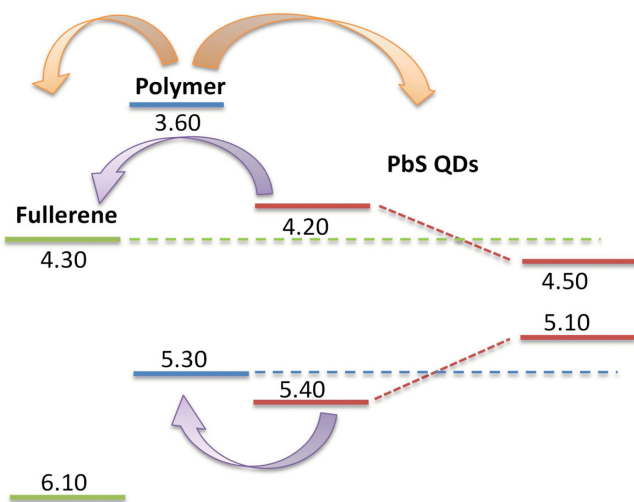

Figure 3. Schematic of the approximate energy-level alignment of the studied materials.

or nonfluorescent. In combination with time-resolved luminescence, which can directly probe interfacial exciton recombination and extend the time probing range to hundreds of nanoseconds, the two techniques provide a precise method to evaluate the excitation dynamics within the films studied. **Figure 4**d shows the maximum differential transmission occurring at zero pump–probe delay for a pump of 400 nm and probe wavelengths in the 500–1100 nm range, for the pristine Si–PCPDTBT, ca. 2.9 nm QD, and the hybrid film of the two materials. For the QD film, negative signals indicating photo-induced absorption to higher lying states are observed apart from the region in the vicinity of the 900 nm, coincident with the 1s states of the dots (see Table 1), where a positive signal indicates that such states are partially occupied. For the pristine polymer, a high positive differential transmission, observed in the 550–800 nm range, is attributed to the photobleaching of the singlet exciton states. The peaks observed energetically match, within the low resolution of the plot, the corresponding steady-state absorption vibronics of Figure 1. The negative data observed at polymer subgap energies have been previously attributed to photoinduced polaron absorption.[31] The spectral characteristics and magnitude of the transient signal from the hybrid film in the 500–800 nm region is very similar to those of the polymer film. This indicates that predominantly polymer exciton states are probed in this region. At polymer subgap energies (850–1100 nm), the hybrid signal appears as a convolution of the negative absorption signal due to polymer polarons and the positive photobleaching of the core QD states. This phenomenon can be readily observed in the differential transmission curves of Figure 4c. The decays at 900 nm of both 2.9- and 6.8-nm QD–polymer films acquire a behavior in between that of the polymer and the respective QDs transients.

Based on the above, two clearly separate spectral regions are defined: i) the 500–800 nm dominated by polymer exciton states and ii) the 850–1100 nm where polymer polaron and QD core and/or surface states are probed. The mixing of the probed states in the latter region with simultaneous observation of linear polymer relaxation and nonlinear QD Auger recombination effects complicates the analysis. Therefore, for the rest of the discussion, our analysis focuses on the 500–800 nm spectral range. The transient behavior in this region is dominated by first-order relaxation as indicated by the approximately linear dependence of the transient peak signals with excitation density (see Supporting Information, Figure S1). Differential transmission transients require multi- (three) exponential decay fits, with an ultrafast sub-picosecond component, a fast decay in the 1–10 ps range, and a considerably slower component in the 0.4–4 ns range. The decays are dominated by the two fast decays with a relative amplitude of 75–85% compared to the slower component. Comparison with the pristine polymer relaxation is obtained by normalized differential transmission curves such as those displayed in Figure 4, containing the decays of the pristine polymer and hybrid films with ca. 2.9 nm QDs and ca. 6.8 nm for probes of 650 and 750 nm. At both wavelengths, the decays from the hybrids are faster than those of the pristine films within the first 10 ps (see the Figure insets). The presence of faster decays in this temporal range is consistently observed in all hybrid films and indicates that in addition to intrinsic polymer relaxation, new recombination channels such as charge and energy transfer
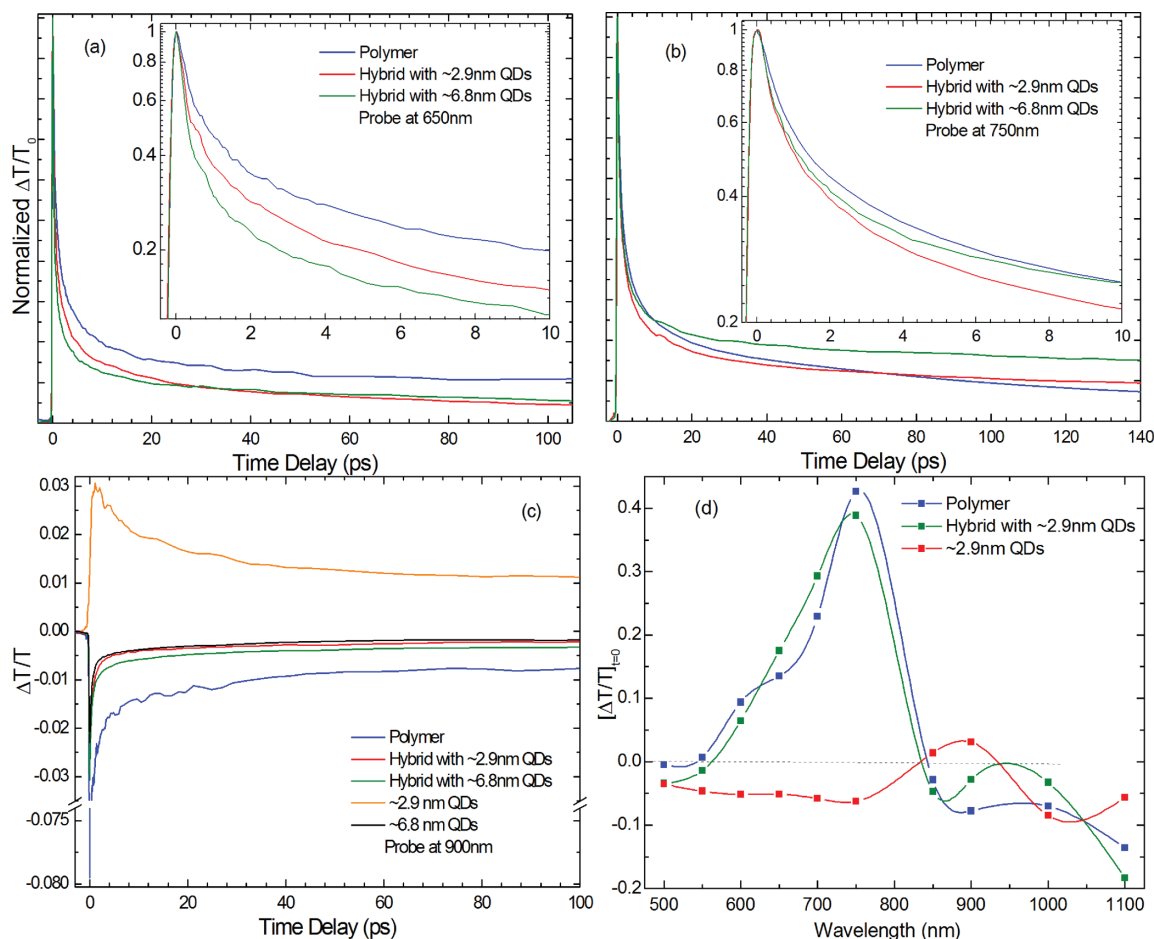
Materials
Views
www.MaterialsViews.com

ADVANCED
ENERGY
MATERIALS
www.advenergymat.de

FULL PAPER

Figure 4. Normalized differential transmission from the pristine polymer and hybrid films with ca. 2.9- and 6.8-nm QDs, at probes of a) 650 nm and b) 750 nm. c) Differential transmission of the pristine and blend materials at 900 nm. d) Maximum differential transmission at zero pump–probe delay for the polymer, ca. 2.9 nm QDs, and the hybrid film of the two. The lines between data are added as a guide to the eye. Below 800 nm the behavior of the hybrid film is dominated by polymer effects while at longer wavelengths, a mixture of polymer polarons and core QD states are probed.

or recombination to trap states induced by the materials' mixing are active in the blends. The ultrafast scales of the effect and the fact that no systematic correlation with QD size was observed, despite the apparent such trend in the graphs of Figure 4a and 4b, are indicative of nonradiative recombination to interfacial defect states formed within the blends. The presence of significant interfacial defect recombination has been hinted in other reports of polymer–PbS QD hybrids[17,32,33] but the timescales of such processes were not previously estimated.

At longer times the hybrid transients show different behaviors dependent on probe wavelength. Systematic trends can be obtained only in the vicinity of the maximum Si–PCPDTBT absorption, at probe wavelengths of 700–750 nm where the hybrids exhibit slower decays in the ca. 1–4 ns range compared to 0.5–1 ns of the pristine polymer. This behavior typically results in crossovers of the polymer and hybrid transient signals such as those seen in Figure 4b. Interestingly a rather systematic trend can be observed, with decays becoming slower as the QD size in the blends increases, as can be seen in Figure 4b. The slow component of Si–PCPDTBT transient absorption signal has been previously attributed to radiative recombination of the Frenkel exciton.[31] The significantly longer decays observed in

the hybrids indicate that in addition to excitons, other longer-lived species are formed in the presence of the QDs. Signatures of long decays of similar timescales and in the same spectral region have been obtained in the pump–probe and time-resolved photoluminescence (TR-PL) spectra of bulk heterojunctions of Si–PCPDTBT with PCBM acceptors,[31] which suggests the presence of long-lived holes and/or charge-transfer excitons. In our case the TR-PL transients presented later in the manuscript do not contain such long decays, which indicates that the long-lived species are nonemissive. Thus these transients can be predominantly attributed to positive polarons formed subsequent to electron-transfer processes to the QDs. This conclusion is consistent with the dependence of the decays on nanocrystal size, as larger dots result in greater energy differences between the LUMO levels of the materials (see Figure 3) that could promote more efficient electron transfer to the QDs.

2.4. Photoluminescence Quenching

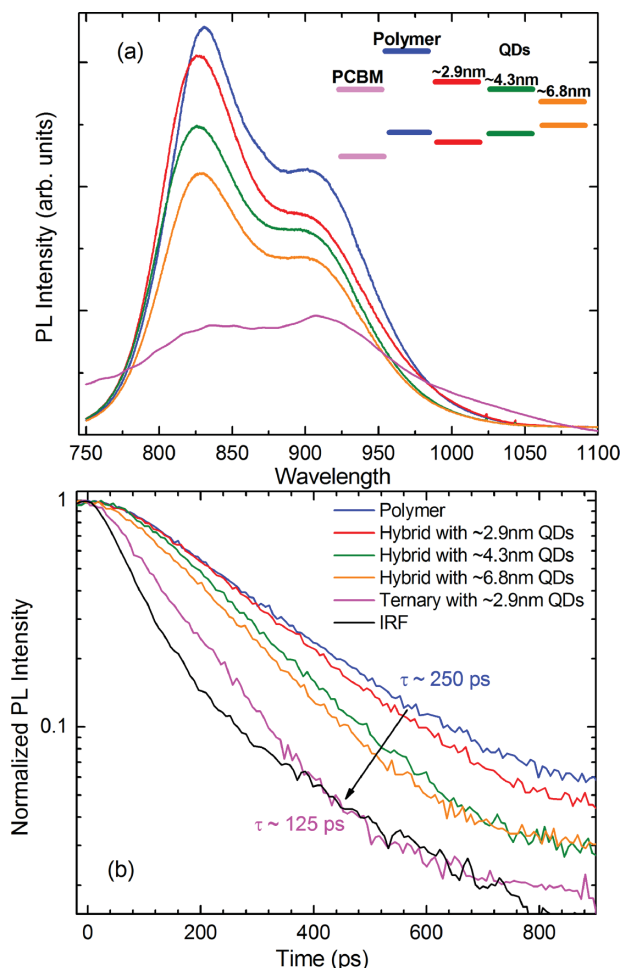Pump–probe measurements provide evidence of intermaterial charge-transfer processes. Steady-state and time-resolved

FULL PAPER

Figure 5. Comparative a) steady-state and b) time-resolved fluorescence spectra in the emission region of Si–PCPDTBT, from the pristine polymer, three polymer–QD blends employing QDs of ca. 2.9, 4.3, and 6.8 nm in size and a ternary polymer–fullerene–QD film based on the ca. 2.9-nm QDs. The instrument response function (IRF) is shown in black.

luminescence adds to this discussion, by monitoring the fluorescence quenching in the blends relative to the pristine films. Initially fluorescence quenching in the polymer emission region is discussed. For both steady-state and time-resolved experiments, the 690-nm line of a laser diode is employed to resonantly excite the polymer component at its absorption peak. In the blend films, 690-nm light results in the selective excitation of the Si–PCPDTBT component, as evidenced by the extremely weak QD luminescence observed in the hybrid spectra. The lack of emission from the quantum dots upon polymer photoexcitation also excludes the possibility of efficient radiative pumping and/or nonradiative Förster[34] energy transfer from the polymer to the QDs. The results are in agreement with previous work on P3HT–PbS QD hybrid blends.[32]

Figure 5 shows the comparative steady-state and time-resolved fluorescence spectra from the pristine polymer, three polymer–QD blends employing QDs of ca. 2.9-, 4.3-, and 6.8-nm in size, and a ternary polymer–fullerene–QD film based on the ca. 2.9-nm QDs. The polymer fluorescence contains

characteristic vibronic peaks at around 830 and 905 nm. Compared to the pristine emission, no significant shape variations are observed in the binary hybrids apart from a small vibronic blue-shift of about 5–10 nm. The origin of the shifts will be discussed later. The ternary film shows a broader emission than the rest of the films, with different relative vibronic intensities indicative of structural interactions induced by the fullerene, and excess emission in the infrared that could be due to charge transfer excitons formed at the Si–PCPDTBT–PCBM interfaces.[31] The main observation is that the hybrid fluorescence quenches relative to the pristine polymer emission, and that the quenching in the polymer–QD films systematically increases with QD size. This trend agrees with the findings of the pump–probe experiments and is consistent with polymer exciton quenching via interfacial electron transfer to the QDs that becomes more efficient as larger QDs result in larger material LUMO separations. This clear QD size correlation also excludes that dielectric effects or trap-related recombination are responsible for the emission reduction. As evidenced by both the intensity and lifetime quenching, electron transfer appears relatively inefficient in comparison to the fast (ca. 250 ps) intrinsic polymer exciton recombination. A simple estimation of the electron transfer rates can be obtained by the difference between the blend (τ_{blend}^{-1}) and pristine ($\tau_{pristine}^{-1}$) exciton recombination rates as given by Equation (3):

$$\tau_{transfer}^{-1} = \tau_{blend}^{-1} - \tau_{pristine}^{-1} \Rightarrow \tau_{transfer} = \frac{1}{\tau_{transfer}^{-1}} \qquad (2)$$

For the larger quenching case of the ca. 6.8-nm QD binary film that exhibits a lifetime of around 190 ps, a relatively long electron-transfer time of about 800 ps is estimated. The addition of even a small blend content of 17 wt% PCBM significantly increases the exciton dissociation rate by providing efficient fullerene quenching sites in the blends. A ternary film decay of ca. 125 ps is measured and an electron-transfer rate of 250 ps is estimated, which competes efficiently with the polymer exciton lifetime. Higher electron-transfer rates from the polymer–dot films may be obtained via mild QD ligand-exchange processes such as those reported in recent demonstrations of efficient polymer–PbS QD solar cells.[15–20]

QD emission quenching was also investigated to probe charge transfer originating in the QDs. In the steady-state experiments the PL was quasi-resonantly excited at 850 nm so excitations were photogenerated solely in the QD component of the blends. Despite the QD low absorption coefficients at 850 nm, strong nanocrystal luminescence was observed that attests to the high quality and emission yield of the materials. PL peaks in the ca. 1050–1400 nm region, with Stokes shifts in the range of 50–170 meV range that increase with nanocrystal size, were observed from the QDs of 2.9–4.3 nm in size. The steady-state and time-resolved PL spectra from the respective QD solutions are included in the Supporting Information, Figure S2a and b. The PL from the two larger dots, i.e., the ca. 6.8 and 9.2 nm size dots, could not be measured due to the very weak response of our infrared photomultiplier tube above 1700 nm. The hybrid PL exhibits similar spectral shape and Stokes shifts with the pristine PL, with peaks consistently blue-shifted by 20–40 meV. As mentioned above, blue shifts are also
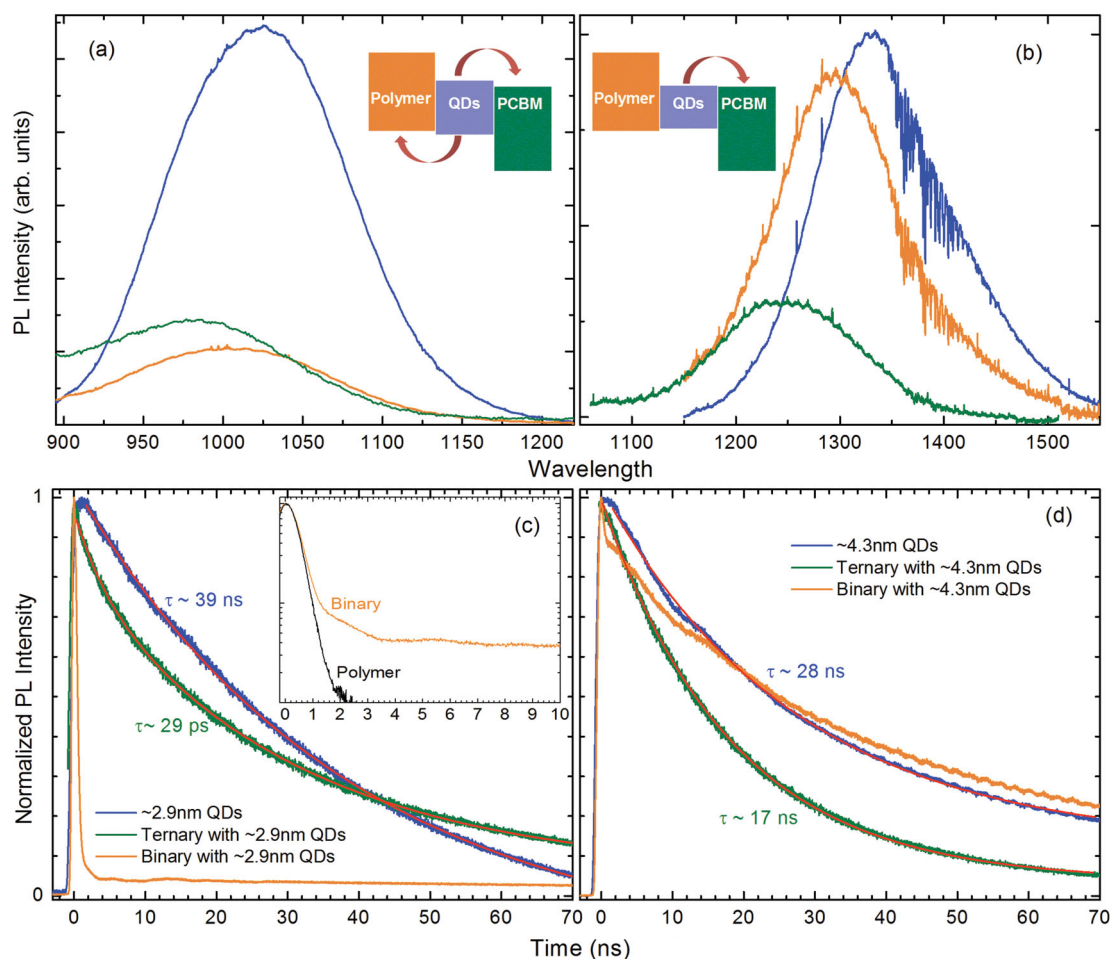
Materials
Views
www.MaterialsViews.com

ADVANCED
ENERGY
MATERIALS
www.advenergymat.de

FULL PAPER

Figure 6. a,b) Steady-state and c,d) time-resolved PL quenching data from pristine QD (blue), binary polymer–QD (orange), and ternary polymer–fullerene–QD films (green). a,c) refer to films based on 2.9-nm QDs while b,d) were on 4.3-nm QDs. Pristine and ternary decays are fitted by double-exponentials (red lines) dominated by the lifetimes displayed in the graph. The inset shows the polymer and binary QD film decays recorded at the peak of the hybrid PL.

present in the Si–PCPDTBT hybrid emission region. Hypsochromic shifts have been observed in binary and ternary combinations of organics such as polythiophenes/fullerenes[32,33] and carbon nanotubes[35] with PbS NCs and have been attributed to either dielectric effects due to the high organic/inorganic dielectric contrast or charge-transfer interactions within the blend materials. We have found no correlation of the shift magnitude with QD size that would imply a correlation with charge-transfer interactions so dielectric effects are the most probable origin of these shifts.

The main observation of the steady-state experiments is the appearance of QD emission quenching indicative of interfacial hole transfer originating in the PbS dots. Importantly the PL quenching systematically decreases as QD size increases, showing the inverse relationship to that observed in the polymer region. Two characteristic examples are displayed in **Figure 6**. The hybrid film made by employing the smaller dots (2.9 nm) exhibits a highly efficient quenching of the QD emission that indicates the formation of type II polymer–dots band alignment. On the other hand, a negligible emission reduction is observed from the hybrid based on the 4.3-nm QDs that is

indicative of a crossover to type I energetic alignment. The incorporation of a small fullerene fraction does not vary emission quenching significantly in the small dot hybrid, while it improves it significantly in the larger dot blend, as an interfacial electron-transfer channel to the fullerene component becomes available. The time-resolved data support the steady-state findings, even though their analysis is more involved due to the unavailability of a proper infrared picosecond source that selectively pumps the QD component. Instead a 375 nm laser was used that excites both polymer and QD components. The ca. 2.9-nm QD binary film transient appears dominated by a fast decay with lifetime of about 400 ps. Comparison of this decay channel with the fluorescence decay of the pristine polymer film recorded in the same energy position shows almost identical decay curves to those in the inset of Figure 6. In combination with the PL excitation-dependent studies summarized in the Supporting Information (Figure S3), the measurements convincingly demonstrate that the sub-nanosecond fast decay originates in the polymer component of the hybrid film. The QDs within the hybrid film contribute with a weak, long decay of about 70 ns, which is significantly longer than the pristine

ADVANCED
ENERGY
MATERIALS
www.advenergymat.de

www.MaterialsViews.com

FULL PAPER

QD decay of around 40 ns. Importantly the relative amplitude of this slow decay is more than one order of magnitude smaller than that of the fast decay, which is a strong indication that in the hybrid film the emission of QDs is strongly quenched as hole transfer to the polymer competes favorably with the intrinsic QD recombination. This result indicates that for small-enough QDs the hole-transfer time assumes values much smaller than those of the pristine QD lifetime (ca. 40 ns) and order(s) of magnitude smaller to typical hole-transfer times of hundreds of nanoseconds reported from similar-sized oleic acid capped PbS QDs to conventional polymers such as P3HT.[33] As the QD size increases in the hybrid films, a systematic trend is observed where the decay attributed to QDs acquires a larger relative amplitude with a lifetime approaching the corresponding pristine QD lifetime. In the larger 4.3-nm dots, the temporal characteristics of the hybrid decay become comparable to those of the pristine QD film due to inhibition of the hole-transfer process.

Based on the results of the binary films, the complex behavior of the ternary films can be understood. Both the 2.9- and 4.3-nm QD ternary films show an efficient QD lifetime shortening. In the former, both hole/electron transfer to the polymer/fullerene component, respectively, are responsible for the quenching, while only electron transfer is expected to be active in the latter film. Despite the approximately flat LUMO alignment[36] of the ca. 4.3-nm QDs and PCBM, a high lifetime quenching is observed that indicates relatively fast electron transfer to the fullerene. Interestingly the ternary decays do not contain the fast sub-nanosecond contribution of the polymer which confirms that the incorporation of even a low fullerene content in the blends is sufficient to efficiently quench the Si–PCPDTBT excitons.

An overall picture of the electron/hole-transfer efficiency versus QD size in the binary and ternary films can be obtained in the summary plot of **Figure 7**. To quantify the emission quenching, the following ratios are defined:

$$Quenching\ Ratio: R_{Intensity} = \frac{I_{pristine} - I_{blend}}{I_{pristine}},$$

$$R_{Lifetime} = \frac{\tau_{pristine} - \tau_{blend}}{\tau_{pristine}} \tag{3}$$

where $R_{Intensity}$ quantifies the steady-state quenching experiments with $I_{pristine}$ and I_{blend} being the integrated PL intensity from the pristine and blend samples, respectively, and $R_{Lifetime}$ defines the PL lifetime quenching with $\tau_{pristine}$ and τ_{blend}, the emission lifetimes from pristine and blend samples, respectively. The two ratios can be considered as a relative measure of the electron/hole-transfer efficiencies in the blends. In Figure 7, the inverse correlation of the electron- and hole-transfer efficiency with the QD size is visible. Time-resolved data in the
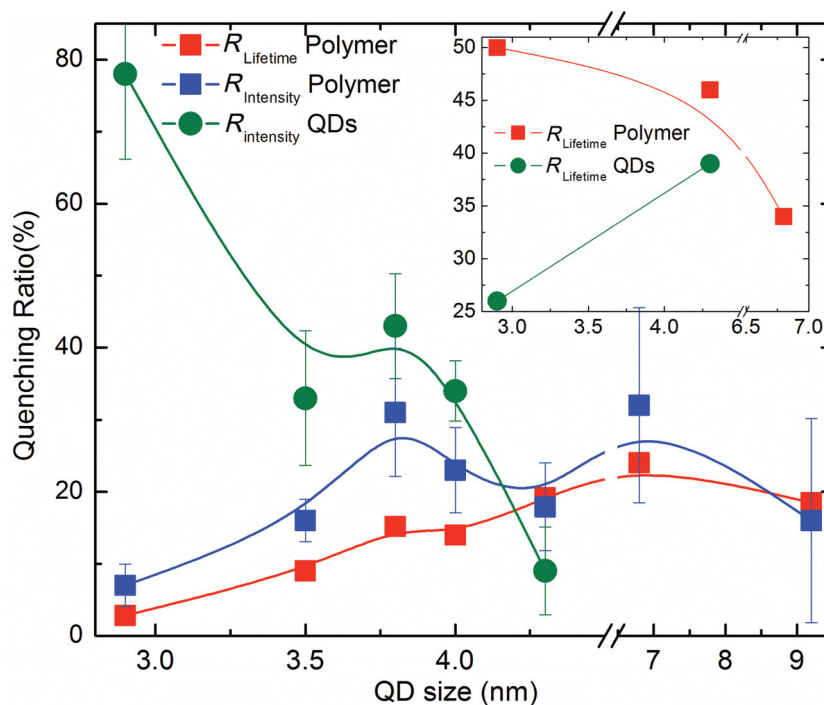

Figure 7. Summary of the steady-state and time-resolved PL quenching experiments for the polymer–QD blends. The error bars denote the standard deviation of $R_{Intensity}$ across the films surface. The inset shows the quenching ratios for the ternary films studied. The lines in the Figures are added as a guide to the eye. In the binary films the inverse dependence of the electron and hole-transfer efficiency with the QD size is visible.

QD region are not included as they cannot be quantified using the simplistic approach of Equation (4). For small dots the data indicate a high hole extraction to the polymer despite the use of the bulky oleic acid ligands. As the QD size increases $R_{Intensity}$ drops due to the inhibition of the hole transfer by unfavorable HOMO polymer–dot band offsets. Electron transfer from the polymer shows a weaker correlation with size and appears less efficient than hole transfer for dots up to 4–4.5 nm despite the presence of significantly larger LUMO compared to the respective HOMO polymer–QD band offsets. The lower efficiency is probably a combination of the high energy required to dissociate the polymer Frenkel exciton as well as the unfavorable competition of the electron-transfer rates with the fast intrinsic polymer exciton recombination. In the inset, of Figure 7 the results from the time-resolved characterization of the ternary films in both polymer and QD regions are included. No reliable trends with QD size can be obtained due to the small number of ternary films, however a higher degree of polymer quenching can be readily observed which can attributed to the presence of PCBM that quench polymer excitons more efficiently than QD acceptors.

3. Conclusions

We have performed a systematic photophysical investigation of blend heterojunctions of the low-gap silicon-bridged dithiophene copolymer Si–PCPDTBT with oleic acid capped PbS

www.MaterialsViews.com

ADVANCED
ENERGY
MATERIALS
www.advenergymat.de

FULL PAPER

QDs. The influence of quantum-dot size on the charge extraction was for the first time explored in a low-gap polymer–PbS QD composite. Pump–probe experiments indicate that a fraction of the hybrid excitations recombine ultrafast on timescales of about 10 ps, most probably at interfacial defects. Emission quenching was found to be dependent on QD size, showing opposite trends in the polymer and QD emission regions. The behavior indicates a quenching emission channel that is strongly influenced by the materials' energy-level alignment. As radiative/nonradiative energy transfer appears inefficient, we can predominantly attribute the quenching to intermaterial charge-transfer processes. For nanocrystal sizes up to around 4–4.5 nm we have found evidence of polymer–dot energetic alignment suitable for light harvesting. For the smallest employed dots of ca. 3 nm, an almost complete quenching of the QD emission indicates the presence of efficient hole transfer to the polymer despite the use of insulating capping ligands. This feature is particularly important as hole transfer in bulk heterojunctions of polymer donors with quantum dots has been typically inefficient. Our results are in agreement with recent studies on hole-transfer dynamics in low-gap polymer–PbS QD blends.[20] Evidence of electron transfer from the polymer was also observed although such transfer competes less efficiently with the intrinsic polymer recombination for most QD sizes studied. The incorporation of a fullerene derivative was found to provide efficient quenching sites that improve polymer exciton dissociation in ternary polymer–fullerene–QD blends, in agreement with previous studies on P3HT-based ternaries.[32,33] A possibly better alternative to ternary blends may be the successful employment of postfabrication ligand-exchange processes which should enable the simultaneous activation of efficient electron and hole extraction, making the Si–PCPDTBT–PbS QD system a promising system for hybrid solar cells and infrared sensors.

4. Experimental Section

Sample Preparation: Si–PCPDTBT was purchased from Konarka Technologies GmbH. The material is a high-performance Si-bridged dithiophene copolymer[25] that exhibits a near-infrared bandgap, planar conformation, and high carrier mobilities attributed to the extended π-delocalization induced by the silicon bridges. Recently it has been employed in bulk heterojunctions with fullerenes showing solar cell power conversion efficiencies larger than 5%.[25,27] Oleic acid capped PbS nanocrystals absorbing in the 900–2000 nm range were synthesized according to methods reported in the literature.[37] The use of the long oleic acid ligands ensured high material quality and stability and relatively good film homogeneity. Post-film fabrication, chemical reactions to replace the QD oleic acids with shorter ligands via organic dithiol treatments such as 1,4-benzenedithiol (BDT)[4] were attempted but found to degrade the material, causing film cracking as the shorter ligands cannot fill the space taken up by the long oleic acid ligands.[38] For the ternary blends, the fullerene derivative phenyl-C60-butyric acid methyl ester (PC$_{60}$BM), purchased from Solenne BV, The Netherlands, was used.

All polymer–fullerene–quantum dot solutions were stirred separately overnight in chlorobenzene and combined several hours before deposition. Solutions were prepared at a fixed total concentration of 30 mg mL^{-1}. Binary polymer-QD combinations were all blended in a ratio of 1:2 per weight (i.e. a 67% QD wt). The same organic to QD ratio was used for ternary films, resulting in a ratio of 1:1:4 (wt:wt:wt)

polymer:fullerene:QDs. The composition was chosen based on optimization studies of previously reported hybrid photodiodes.[24] Hybrid solar cells require in general higher QD loadings up to 90% wt[15–20] however the simultaneous tuning of the QD size and blend in a wide range is impractical so the influence of the latter will be studied elsewhere. Binary and ternary films as well as reference pristine nanocrystal and polymer films were deposited on quartz substrates using a doctor-blade technique under ambient conditions. Film thicknesses ranged from 400–600 nm as measured with a Dektak profilometer.

Electrochemistry: Experiments were performed using a standard three-electrode cell under argon atmosphere. All measurements were carried out with 10–15 mins of Ar bubbling into the electrochemical cell. Prior to the measurements, the Ar flow was turned to "blanket-mode". Platinum wire (99.99%) was used as working electrode and platinum gauze (55 mesh, 99.9%) as counter electrode. Silver/silver chloride was used as a reference electrode. Tetrabutylammonium hexafluorophosphate (TBAPF6, 98%) was used as electrolyte and was recrystallized three times from acetone and dried in vacuum at 100°C before each experiment. Measurements were recorded using a potentiostat/galvanostat. The scan rate was kept constant for all voltammograms at 100 mV s^{-1}. All results were calibrated using commercially available ferrocene (purified by sublimation) as internal standard. To calculate HOMO/LUMO levels, the following equations were used:

$$E_{HOMO} = -(E_{[ox]} + 5.1)\,(eV), \quad E_{LUMO} = -(E_{[red]} + 5.1)\,(eV) \qquad (4)$$

where $E_{[ox]}$ and $E_{[red]}$ are the onset potentials of the respective oxidation and reduction peak signals.[39]

Optical Spectroscopy: Film absorption was carried out using a three-detector UV/Vis/NIR spectrophotometer. Steady-state photoluminescence (PL) was performed using a high resolution 0.75 m spectrometer equipped with a charge-coupled device (CCD) camera and an InGaAs array detector. The PL was excited using chopped (100 Hz) lines of three continuous wave (cw) laser diodes emitting at 850, 690, and 375 nm, chosen to selectively excite the QDs, the polymer or both of the two blend components, respectively. Time-resolved PL was measured using a 0.35 m spectrometer-based time-correlated single-photon counting (TCSPC) system, equipped with a visible and an infrared photomultiplier tube (PMT) that covers the 250–1700 nm range. The PL was excited by a 375 or a 690 nm picosecond laser diode adjusted to repetition rates of 100 KHz–1 MHz. The system exhibits a time-resolution of ca. 50 ps (visible PMT)/100 ps (infrared PMT) after reconvolution with the instrument response function. The PL quenching measurements were performed on side-by-side sample geometry to allow a direct emission-intensity comparison. Furthermore the laser fluence was normalized to the optical absorbance (optical density) of each sample at the excitation wavelength used to approximately photogenerate an equal density of excitations at all films. The PL quenching ratios were obtained by the integrated emission average of six different spots across each sample surface, with the standard deviation of the measurements defined as their error. All PL data were acquired with samples placed in vacuum conditions (ca. 10^{-3} mbar), while moderate to low excitation densities in the 10–100 mW cm^{-2} range were used to avoid material photodegradation.

For the time-resolved transmission, mode-locked pulses of ca. 100 fs from an 800 nm oscillator served as the seed for a regenerative amplifier to produce about 150 fs output pulses of 1 mJ pulse^{-1} with a 1 kHz repetition rate. Measurements were carried out using a typical pump–probe optical setup in a non-colinear configuration. A nonlinear second harmonic BBO crystal was used to obtain excitation pulses at 400 nm. In addition, white light continuum pulses in the region between 500–1100 nm were generated in a sapphire crystal and used as the probe pulses. The probed wavelength was selected by means of appropriate bandpass filters. The time delay between the two pulses was achieved via a computer-controlled translation stage with special resolution of 0.1 μm. During the experiments the samples were mounted into a nitrogen flow-through cell and kept under nitrogen atmosphere.

FULL PAPER

Supporting Information

Supporting Information is available from the Wiley Online Library or from the author.

Acknowledgements

[1] C. J. Brabec, S. Gowrisanker, J. J. M. Halls, D. Laird, S. Jia, S. P. Williams, *Adv. Mater.* **2010**, *22*, 3839.

[2] A new world record for organic solar technology with a cell efficiency of 12%, http://www.heliatek.com/newscenter/latest_news/neuer-weltrekord-fur-organische-solarzellen-heliatek-behauptet-sich-mit-12-zelleffizienz-als-technologiefuhrer/?lang=en, 16/01/2013

[3] J. P. Clifford, K. W. Johnston, L. Levina, E. H. Sargent, *Appl. Phys. Lett.* **2007**, *91*, 253117.

[4] K. Szendrei, W. Gomulya, M. Yarema, W. Heiss, M. A. Loi, *Appl. Phys. Lett.* **2010**, *97*, 203501-1.

[5] A. G. Pattantyus-Abraham, I. J. Kramer, A. R. Barkhouse, X. Wang, G. Konstantatos, R. Debnath, L. Levina, I. Raabe, M. K. Nazeeruddin, M. Grätzel, E. H. Sargent, *ACS Nano* **2010**, *4*, 3374.

[6] J. Tang, H. Liu, D. Zhitomirsky, S. Hoogland, X. H. Wang, M. Furukawa, L. Levina, E. H. Sargent, *Nano Lett.* **2012**, *12*, 4889.

[7] J. Xiao, Y. Wang1, Z. Hua, X. Wang, C. Zhang, M. Xiao, *Nat. Commun.* **2012**, *3*, 1170.

[8] J. Huang, Z. Huang, Y. Yang, H. Zhu, T. Lian, *J. Am. Chem. Soc.* **2010**, *132*, 4858.

[9] N. C. Greenham, X. Peng, A. P. Alivisatos, *Phys. Rev. B* **1996**, *54*, 17628.

[10] W. U. Huynh, J. J. Dittmer, A. P. Alivisatos, *Science* **2002**, *295*, 2425.

[11] M. Wright, A. Uddin, *Sol. Energy Mater. Sol. Cells* **2012**, *107*, 87.

[12] A. J. Moulé, L. Chang, C. Thambidurai, R. Vidu, P. Stroeve, *J. Mater. Chem.* **2012**, *22*, 2351.

[13] Y. Yin, A. P. Alivisatos, *Nature* **2005**, *437*, 664.

[14] S. Ren, L.-Y. Chang, S.-K. Lim, J. Zhao, M. Smith, N. Zhao, V. Bulovic, M. Bawendi, S. Gradečak, *Nano Lett.* **2011**, *11*, 3998.

[15] D. Celik, M. Krueger, C. Veit, H. F. Schleiermacher, B. Zimmermann, S. Allard, I. Dumsch, U. Scherf, F. Rauscher, P. Niyamakom, *Sol. Energy Mater. Sol. Cells* **2012**, *98*, 433.

[16] Y. Zhou, M. Eck, C. Menb, F. Rauscher, P. Niyamakom, S. Yilmaz, I. Dumsch, S. Allard, U. Scherf, M. Krüger, *Sol. Energy Mater. Sol. Cells* **2011**, *95*, 3227.

[17] C. Piliego, M. Manca, R. Kroon, M. Yarema, K. Szendrei, M. R. Andersson, W. Heiss, M. A. Loi, *J. Mater. Chem.* **2012**, *22*, 24411.

[18] J. Seo, M. J. Cho, D. Lee, A. N. Cartwright, P. N. Prasad, *Adv. Mater.* **2011**, *23*, 3984.

[19] Y. Zhang, Z. Li, J. Ouyang, S.-W. Tsang, J. Lu, K. Yu, J. Ding, Y. Tao, *Sol. Energy Mater. Sol. Cells* **2011**, *13*, 2773.

[20] A. E. Colbert, E. M. Janke, S. T. Hsieh, S. Subramaniyan, C. W. Schlenker, S. A. Jenekhe, D. S. Ginger, *J. Phys. Chem. Lett.* **2013**, *4*, 280.

[21] S. Dayal, N. Kopidakis, D. C. Olson, D. S. Ginley, G. Rumbles, *Nano Lett.* **2009**, *10*, 239.

[22] K. M. Noone, E. Strein, N. C. Anderson, P.-T. Wu, S. A. Jenekhe, D. S. Ginger, *Nano Lett.* **2010**, *10*, 2635.

[23] A. L. Rogach, A. Eychmüller, S. G. Hickey, S. V. Kershaw, *Small* **2007**, *3*, 536.

[24] T. Rauch, M. Böberl, S. F. Tedde, J. Fürst, M. V. Kovalenko, G. Hesser, U. Lemmer, W. Heiss, O. Hayden, *Nat. Photonics* **2009**, *3*, 332.

[25] M. C. Scharber, M. Koppe, J. Gao, F. Cordella, M. A. Loi, P. Denk, M. Morana, H.-J. Egelhaaf, K. Forberich, G. Dennler, R. Gaudiana, D. Waller, Z. Zhu, X. Shi, C. J. Brabec, *Adv. Mater.* **2010**, *22*, 367.

[26] M. C. Scharber, D. Mühlbacher, M. Koppe, P. Denk, C. Waldauf, A. J. Heeger, C. J. Brabec, *Adv. Mater.* **2006**, *18*, 789.

[27] M. Morana, H. Azimi, G. Dennler, H.-J. Egelhaaf, M. Scharber, K. Forberich, J. Hauch, R. Gaudiana, D. Waller, Z. Zhu, K. Hingerl, S. S. van Bavel, J. Loos, C. J. Brabec, *Adv. Funct. Mater.* **2010**, *20*, 1180.

[28] J. Hou, H.-Y. Chen, S. Zhang, G. Li, Y. Yang, *J. Am. Chem. Soc.* **2008**, *130*, 16144.

[29] I. Moreels, K. Lambert, D. Smeets, D. De Muynck, T. Nollet, J. C. Martins, F. Vanhaecke, A. Vantomme, C. Delerue, G. Allan, Z. Hens, *ACS Nano* **2009**, *3*, 3023.

[30] W. Brütting, *Physics of Organic Semiconductors Handbook*, Wiley-VCH, **2005**.

[31] A. Othonos, G. Itskos, M. Neophytou, S. A. Choulis, *Appl. Phys. Lett.* **2012**, *100*, 153303.

[32] G. Itskos, A. Othonos, T. Rauch, S. F. Tedde, O. Hayden, M. Kovalenko, W. Heiss, S. A. Choulis, *Adv. Eng. Mater.* **2011**, *1*, 802.

[33] D. Jarzab, K. Szendrei, M. Yarema, S. Pichler, W. Heiss, M. A. Loi, *Adv. Funct. Mater.* **2011**, *21*, 1988.

[34] T. Förster, *Discuss. Faraday Soc.* **1959**, *27*, 7.

[35] D. Wang, J. K Baral, H. Zhao, B. A. Gonfa, V.-V. Truong, M. A. El Khakani, R. Izquierdo, D. Ma, *Adv. Funct. Mater.* **2011**, *21*, 4010.

[36] A. Gocalinska, M. Saba, F. Quochi, M. Marceddu, K. Szendrei, J. Gao, M. A. Loi, M. Yarema, R. Seyrkammer, W. Heiss, A. Mura, G. Bongiovanni, *J. Phys. Chem. Lett.* **2010**, *1*, 1149.

[37] M. A. Hines, G. D. Scholes, *Adv. Mater.* **2003**, *15*, 1844.

[38] G. Sarasqueta, K. R. Choudhury, F. So, *Chem. Mater.* **2010**, *22*, 3496.

[39] C. M. Cardona, W. Li, A. E. Kaifer, D. Stockdale, G. C. Bazan, *Adv. Mater.* **2011**, *23*, 2367.